Faculty of Science

University of South Bohemia in České Budějovice

Mechanism of Energy Conversion in ATP Driven Molecular Machines: Development of Single-molecule Techniques for Observation of Conformational Changes in Sec Translocon during Protein Transport

Bachelor Thesis

Edrin Sulejmani

Supervisor: Joel Crossley, Ph.D.

Co-Supervisor: Tomáš Fessl, Ph.D.

České Budějovice, 2022

Sulejmani, E. 2022: Mechanism of Energy Conversion in ATP Driven Molecular Machines: Development of Single-molecule Techniques for Observation of Conformational Changes in Sec Translocon during Protein Transport. Bc Thesis, in English - 32 p., Faculty of Science, University of South Bohemia, České Budějovice, Czech Republic.

Annotation:

Optimization and application of single molecule detection techniques for the investigation of the SecA conformational dynamics.

Declaration

I declare that I am the author of this qualification thesis and that in writing it I have used the sources and literature displayed in the list of used sources only.

Place, Date

České Budějovice, 16.08.2022

Signature

Acknowledgment

My sincerest gratitude goes to my supervisor Joel Crossley, Ph.D., for his continuous assistance in the laboratory and computational work, and his tremendous patience.

Acknowledgment goes to my co-supervisor Tomáš Fessl, Ph.D., for his support throughout the thesis and for carrying the work of this thesis in his laboratory.

Special appreciation goes to my family, for emotional and financial support through this academic journey.

Abstract

Translocation of the unfolded proteins across the inner cell membrane in gram-negative bacteria is mediated by SecA, an ATPase protein in complex with the membrane channel known as SecYEG. Although this is a vital bacterial pathway, the mechanism of translocation remains unclear. In this thesis, the conformational space of SecA was investigated in the presence of ADP, ATP, SecYEG, and polypeptide pre-protein Spy (pSpy) using ensemble and single-molecule fluorescence resonance energy transfer (sm-FRET) methods. Ensemble FRET measurements show no changes in SecA state (in absence of SecYEG) upon the addition of ATP. There were also no significant changes in the SecA with pSpy alone. However, in the presence of the pSpy and ATP small conformational changes were observed, hinting the transition into more closed SecA conformation. This is in agreement with previously published data implying a limited ATPase activity of SecA in the absence of a pre-protein and SecYEG. As high optical collection efficiency and low noise are essential requirements for sm-FRET measurements, to improve these characteristics, the optimization of the focal depth was done.

1 Aim of Project

Despite several models attempting to explain the SecA-mediated translocation of trans-membrane proteins through the SecYEG complex in gram-negative bacterial cells, there is still no clear picture of it. The focus of this bachelor thesis is the optimization and application of single molecule detection techniques for the investigation of the aforementioned quest.

2 The Biological System

2.1 Sec Translocon

2.1.1 Structure and Function of the SecYEG Complex

SecYEG is an integral membrane protein complex made of three proteins such as SecY, SecE, and SecG. The main component of this complex is SecY protein, composed of 10 trans-membrane domains, arranged in a pseudo-2-fold symmetry, creating an hour-glass-shaped aqueous channel. The center of this channel, aligned with a long aliphatic residue skeleton, allows the passage of the substrate protein during translocation (Van den Berg et al. 2004; Cranford-Smith and Huber, 2018). SecY contains also a lateral gate, positioned between the halves of the protein, which in the open conformational stage serves to recognize the signal sequence of the substrate protein targeted for translocation (Li et al. 2016; Cranford-Smith and Huber, 2018). Opposite the lateral gate, a "pivot" links two halves of the protein, maintaining its structural integrity (Van den Berg et al. 2004; Cranford-Smith and Huber, 2018). SecE and SecG proteins play an important role in stabilizing the SecY protein (Taura et al. 1993; Nishiyama, Hanada and Tokuda 1994; Cranford-Smith and Huber, 2018).

Structural studies suggest that the SecYEG complex undergoes three conformational transformations: (i) closed, (ii) partially open, and (iii) open conformation (Van den Berg et al. 2004; Zimmer, Nam and Rapoport 2008; Allen et al. 2016; Li et al. 2016; Cranford-Smith and Huber, 2018). The closed state is characterized by the blockage of the aqueous channel from the α-helical plug domain, whereas the partially open and open conformations are the result of the interaction between SecYEG complex and ADP, respectively ATP-bound SecA (Van den Berg et al. 2004; Zimmer, Nam and Rapoport 2008; Allen et al. 2016; Li et al. 2007; Cranford-Smith and Huber 2018). The general structure of the SecYEG complex is depicted in Figure 2.1.
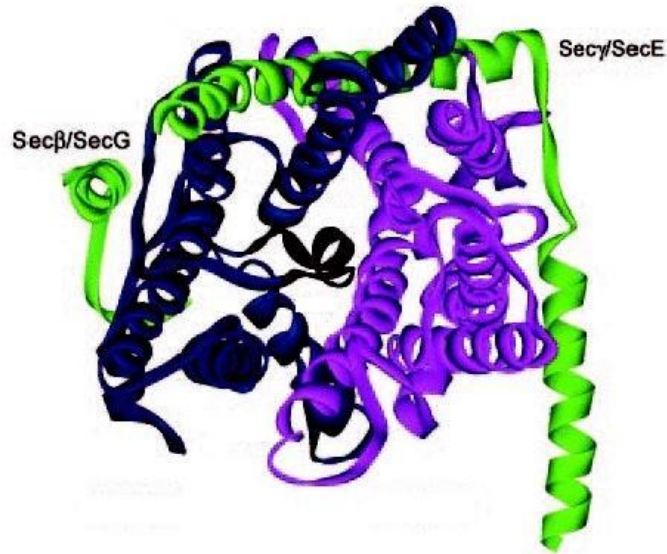
Figure 2.1: SecYEG complex. The two halves of SecY are depicted in dark blue and purple, which form a clamp serving as a passage for trans-membrane protein delivery. The structure is viewed from the periplasmic side (Maillard, Chan, and Duong, 2013).

2.1.2 Structure and Function of the SecA

SecA is a protein, required for the translocation of an abundant percentage of proteins synthesized in *E. coli* (Oliver and Beckwith, 1981; Oliver and Beckwith, 1982; Cranford-Smith and Huber, 2018). Within these cells, SecA has the functional properties of an ATPase, required to catalyze the movement of the substrate pre-protein. ATPase activity of the SecA is observed at the interface between two nucleotide-binding domains, NBD-1, respectively NBD-2 (Schmidt et al. 1988; Lill et al. 1989; Hunt et al. 2002; Cranford-Smith and Huber, 2018). See the structure of SecA in figure 2.2. The primary structure of NBD-1 is discontinued by the polypeptide cross-linking domain (PPDX), whereas on the C-terminal of the NBD-2 is located an α-helical domain comprised of two sub-domains (Hunt et al. 2002; Cranford-Smith and Huber, 2018): (i) the α-helical scaffold domain (HSD) and the α-helical wing domain (HWD). Near the C-terminus of the HSD, a two-helix finger (2HF) domain is located (Erlandson et al. 2008; Cranford-Smith and Huber, 2018). PPXD initiates the contact between SecA and the pre-protein (Bauer and Rapoport 2009; Cranford-Smith and Huber, 2018), whereas the 2HF contacts the pre-protein, playing a crucial role in the translocation process (Erlandson et al. 2008; Cranford-Smith and Huber, 2018).

SecA undergoes large conformational changes upon interaction with SecYEG complex, or a pre-protein (Zimmer, Nam and Rapoport 2008; Chen et al. 2015; Cranford-Smith and Huber, 2018). Specifically the PPXD undergoes large rotational and translational movements resulting in a modulation of the distance between the PPXD domain and the NBD-2. This also affects the distance to HWD (Zimmer, Nam and Rapoport 2008; Chen et al. 2015; Cranford-Smith and Huber, 2018)

The groove between PPXD and NBD-2 is known as a 'clamp' and it is responsible for the binding of the pre-protein. The closed state of the clamp stimulates the ATPase activity (Fak et al. 2004; Gold et al. 2013; Cranford-Smith and Huber, 2018). The closed state occurs when the PPXD is positioned near the NBD-2, whereas the open state is linked with an increased distance from the NBD-2. On contrary, the open state of the clamp means that PPXD moves closer to HWD and the closed state is reflected in the increase in distance between PPXD and HWD.
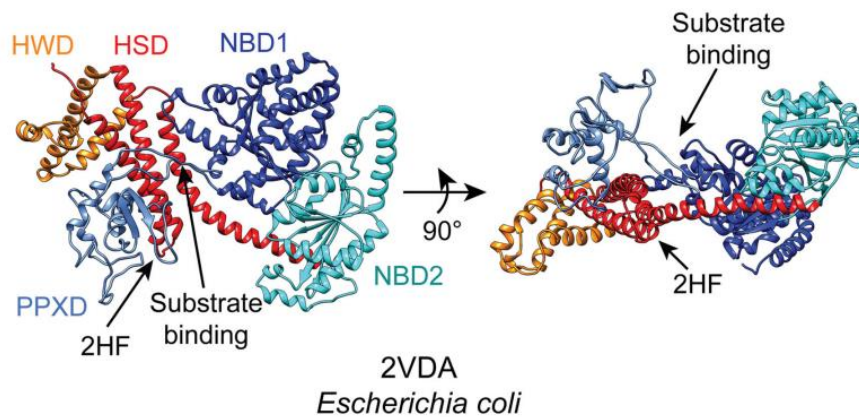

Figure 2.2: The structure of *E. coli* SecA is shown in the open clamp state. In the groove between NBD-1/-2 and PPXD substrate binding occurs (Cranford-Smith and Huber, 2018; Gelis et al., 2007).

2.1.3 SecA-Mediated Protein Translocation Models

The mechanistic models describing the translocation of the substrate proteins through the SecYEG complex are generally classified into three types: (i) processive, (ii) probabilistic, and (iii) mixed processive/probabilistic (Cranford-Smith and Huber, 2018).

Most processive models claim dimerization or oligomerization of the SecA to account for mechanistic requirements for translocation of the substrate protein (Gouridis et al. 2013; Cranford-Smith and Huber, 2018). Multimerization is also suggested given the similarities with RecA helicases, which the latter undergoes to unwind the RNA molecules (Ye et al. 2004; Cranford-Smith and Huber, 2018). The binding of the ATP to the potential SecA dimer increases the interaction affinity with the SecYEG complex and prevents on a certain scale its proteolytic digestion, implying conformational changes (Economou and Wickner 1994; Cranford-Smith and Huber, 2018). These structural transformations further enhance translocation capabilities of the Sec-A (Schiebel et al. 1991; Cranford-Smith and Huber, 2018). The hydrolysis of ATP, and hence the formation of ADP, results in a pre-translocation state of the motor, which may initiate another round of translocation, nevertheless always preventing the backward movement of the substrate protein (van der Wolk et al. 1997; Cranford-Smith and Huber, 2018).

According to the probabilistic models, SecA protein regulates the conformation of the SecYEG complex. Concretely, ADP-bound SecA protein constrains a partially open conformation to the SecYEG complex, allowing only the passage of amino acids with a small side chain. The presence of the selected amino acids is discerned by the SecYEG and 2HF, resulting in a nucleotide exchange reaction, thus forming ATP-bound SecA, which causes the open conformation of the SecYEG and enables the translocation of the substrate protein (Cranford-Smith and Huber, 2018).

In the mixed processive/probabilistic models, the translocation of the substrate protein is described as diffusional, however, the substrate movement is influenced by the 2HF. Respectively, the interaction of SecA with the SecYEG complex causes its open conformation, whereas binding of the former one with ATP enables translation of the 2HF, which initiates the translocation of the substrate protein (Erlandson et al. 2008; Bauer et al. 2014; Cranford-Smith and Huber, 2018). Although this translocation is not sufficient, the largest part is done through simple diffusion (Schiebel et al. 1991; Cranford-Smith and Huber, 2018). A schematic depicting the aforementioned models is depicted in Figure 2.3.
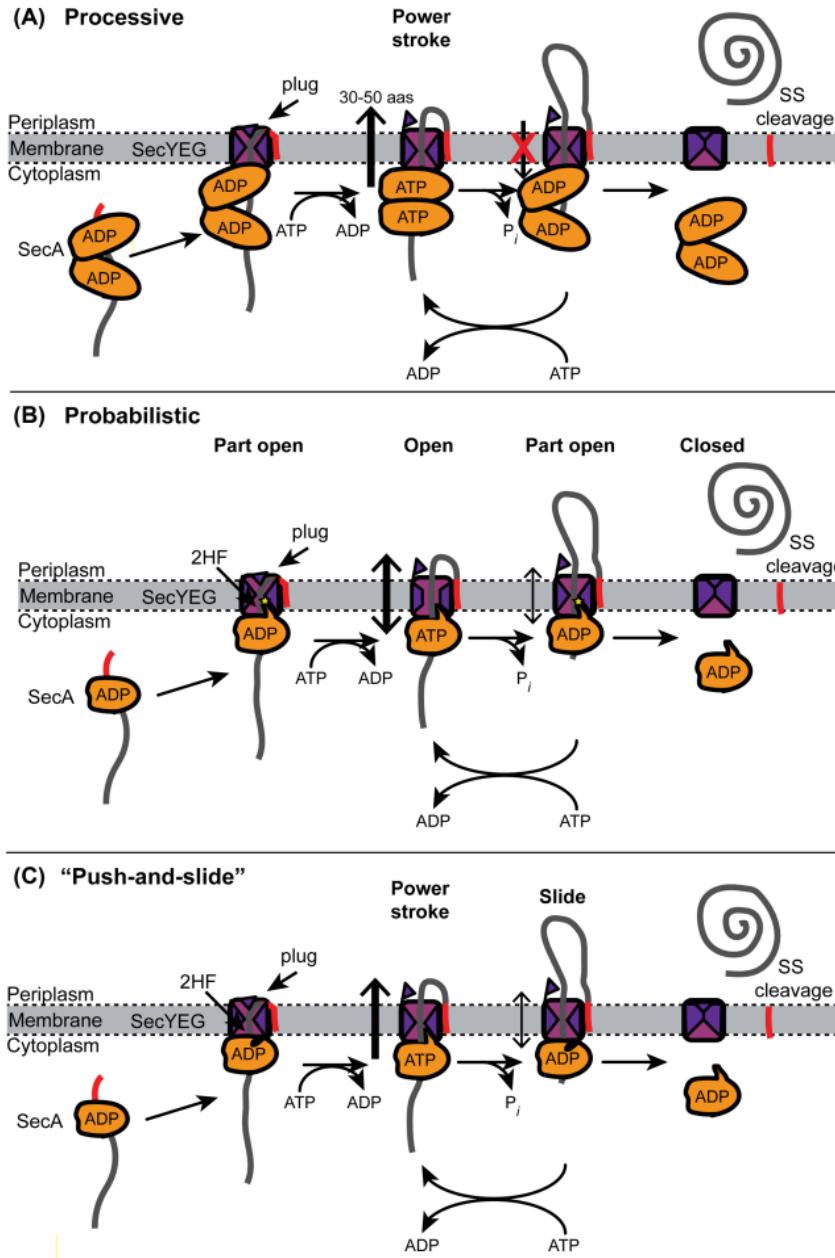
Figure 2.3: Model of SecA-mediated transmembrane protein translocation. (A) Processive models support ATP-stimulated conformational changes in SecA, resulting in its 'open' conformation state, as a requirement for trans-membrane protein translocation. Most models suggest oligomerization of the SecA, to account for such a power-stroke mechanism. ATP to ADP hydrolysis could result in the restoration of the pre-translocation state, or initiation of a second push. (B) Probabilistic models state the formation of the partially-open state of the SecYEG complex when SecA is bound to ADP, where a fully open one is in the presence of ATP. Translocation of the polypeptide is diffusional. (C) Mixed processive/probabilistic models support the hypothesis of a fully open state of the SecYEG complex when SecA is bound to ADP. The binding of ATP causes movement of the 2HF sub-domain, resulting in directional diffusion of the polypeptide through SecYEG (Cranford-Smith and Huber, 2018).

3 Single-molecule Detection Techniques

Single-molecule detection techniques are techniques utilized for observing single molecules, and consequently elucidation of their complex dynamic behaviors and molecular interactions (Miller et al.). An overview of the techniques using light microscopy methods is given here.

3.1 Light Microscopy Approaches

Light microscopy tools are convenient for studying small molecules due to the small perturbation of their native physiological state. Fluorescence emission is mainly used in these techniques, which upon separation of the absorption and the emission wavelength (see Figure 3.1) allows filtering of the excitation wavelength using dichroic mirrors, thus increasing image contrast.

To overcome the optical resolution limit most methods use the photo-physical properties of the fluorophore to achieve low spatial density (Miller et al., "Single-Molecule Techniques in Biophysics: A Review of the Progress in Methods and Applications").
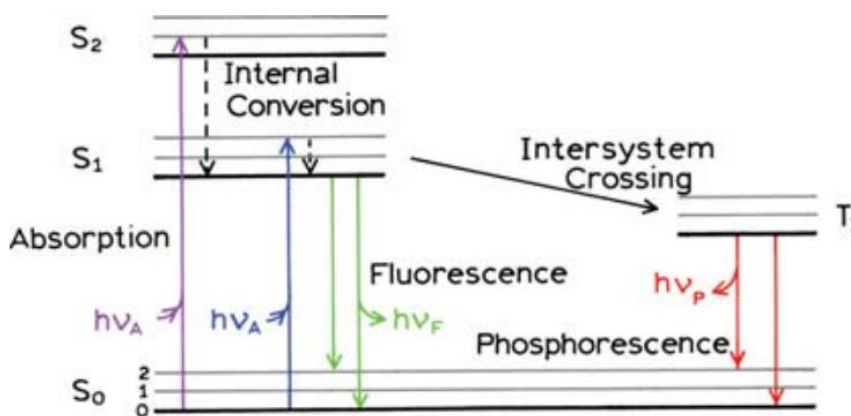

Figure 3.1: Jablonski diagram. Five main processes are shown, starting from left to right, it displays the absorption, internal conversion, intersystem crossing, and phosphorescence from the fluorophore (Lakowicz, *Principles of Fluorescence Spectroscopy*).

3.1.1 Fluorescence Correlation Spectroscopy (FCS)

FCS is a powerful technique used for quantifying molecular dynamics by analyzing time correlation intensity fluorescence fluctuations emitted by bio-molecules upon diffusion through a small observation volume. FCS is commonly implemented in a confocal system, as depicted in Figure 3.2. To enhance the signal-to-noise ratio (SNR) and also reduce the measurement time needed to obtain a decent correlation curve, a femtoliter excitation volume is reached by a high numerical aperture objective combined with epi-fluorescence configuration, *i.e.*, excitation and emission through the same objective, combined with a micro-meter sized pinhole. The fluorescence emitted in the out-of-focus region is rejected by the pinhole, and therefore, it does not reach the detector. After passing through a long-pass dichroic mirror, the fluorescence is focused through a pinhole onto an avalanche photodiode (APD). To further enhance the signal-to-noise ratio, usage of pulsed lasers over continuos-wave (CW), and a time-correlated single-photon counting (TCSPC) for detection, is preferred.
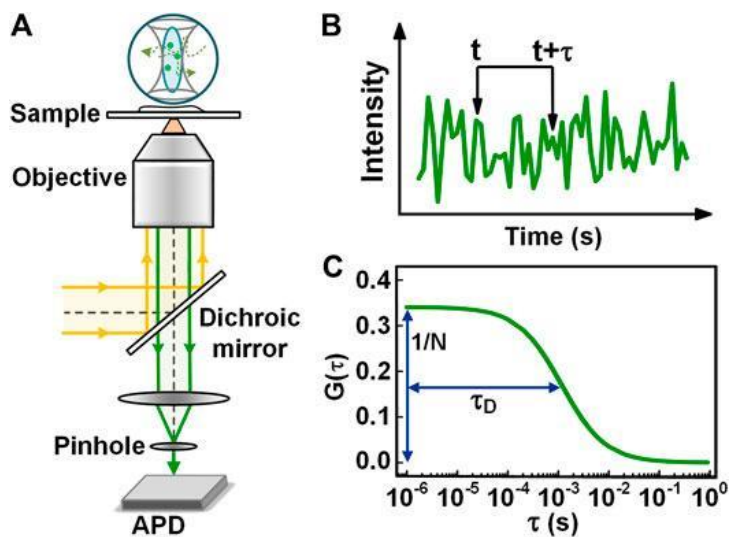

Figure 3.2: FCS. (**A**) Schematic overview of the diffusion-based FCS measurements. (**B**) Fluorescence intensity collected from the observation volume. (**C**) Autocorrelation curve calculated from the fluorescence intensity (Yu et al., "A Comprehensive Review of Fluorescence Correlation Spectroscopy").

Autocorrelation of the intensity fluorescence fluctuation $F(t)$ is calculated as:

$$G(\tau) = \frac{< F(t)F(t+\tau) >}{< F(t) >^2} - 1 \qquad [3.1]$$

where $<>$ denotes the temporal average, τ is the lag time. $G(\tau)$ represents the overlap of the signal with itself at a lag time τ. Such correlation can be made with a computer-based software or hardware correlator. Due to a 3D Gaussian profile of the observation volume, $G(\tau)$ can be fitted with a 3D diffusion model as follows:

$$G(\tau) = \frac{1}{N}(1 + \frac{\tau}{\tau_D})^{-1}(1 + \frac{\tau}{\tau_D} \cdot \frac{r_0^2}{z_0^2})^{-\frac{1}{2}} \qquad [3.2]$$

where N denotes the average number of molecules in observational volume; τ_D is the average time a molecule needs to diffuse through the observational volume; r_o and z_o denote the lateral and axial distances over which the intensity decays $\frac{1}{e^2}$ in the lateral and axial directions, respectively. The ratio $\frac{r_0}{z_0}$ becomes zero, when considering 2D diffusion, such as diffusion of molecules in a membrane, thus giving the expression $G(\tau) \sim \frac{1}{N}$. The width of the correlation curve $\tau_D = r_0^2/(4D)$ represents the average time a molecule diffuses through the focus laterally, where D denotes the diffusion coefficient. Once $G(\tau)$ is fitted with the model in equation 3.2, N and τ_D are obtained, which upon pre-calibration of r_0 can yield D. From D the hydrodynamic radius R_H can be calculated from the expression $R_H = K_B T/6\pi\eta D$, where K_B denotes Boltzmann constant, T the thermodynamic temperature, and η the solution viscosity (Yu et al., "A Comprehensive Review of Fluorescence Correlation Spectroscopy").

3.1.2 FRET

FRET describes distance-dependent, non-radiative, dipole-dipole coupling energy transfer from two light-sensitive molecules (chromophores) (Hohlbein, Craggs, and Cordes, 2014; Pawley and Springer Science+Business Media; Volkhard Helms). To occur, three conditions must be fulfilled: (i) spectral overlap of the emission spectrum of the donor with the absorption spectrum of the acceptor, (ii) the distance between chromophores should be between 2-10 nm, (iii) the dipole moments of the chromophores should not be perpendicular to each other.

The FRET efficiency E can be calculated as follows:

$$E = \frac{k_T}{k_T + k_D} = 1 - \frac{\tau_T}{\tau_D} = \frac{1}{1 + (R/R_0)^6}$$ [3.3]

where k_T denotes the energy transfer rate between donor and acceptor; k_D energy transfer rate of the donor in the absence of the acceptor; τ_T fluorescence lifetime of the donor-acceptor species; τ_D fluorescence lifetime of the donor-only species; R distance between two dipoles, and R_0 the Förster radius which describes the distance between dipoles at E equal to 0.5.

R_0 is calculated as follows:

$$R_0^6 = \frac{9000 \, ln \, ln \, 10 \, \varphi_D k^2}{128 \pi^5 N n^4} \int_0^\infty f_D(\lambda) \varepsilon_A(\lambda) \lambda^4 d\lambda$$ [3.4]

where φ_D is the donor quantum yield in the absence of an acceptor, N is Avogadro's number, n is the refractive index of the intervening solution, and k^2 is the dipole orientation factor, which is equal to 2/3 when both chromophores are in free-rotation. The overlap integral is a function of the wavelength λ and is calculated using ε_A as the molecular extinction coefficient of the acceptor and f_D as the wavelength-dependent emission spectrum of the donor.

To look beyond static and dynamic heterogeneity occurring in biological samples, which are the limit of ensemble-based FRET studies, smFRET analyses are preferably applied. Due to high SNR, diffusion-based confocal microscopy is commonly utilized for such techniques. A scheme of such an experimental setup is depicted in Figure 3.3. As in diffusion-based FCS measurements (see Figure 3.2) an epi-fluorescence configuration is used, and a pinhole to confine to the confocal volume. As opposed to the previously-states setup, two lasers for excitation are used and suitable bandpass filters adapted to the properties of the chromophores used. Usage of two lasers establishes the setup modulation needed for alternating-laser-excitation (ALEX), which alternately directly excites the donor and the acceptor fluorophore during diffusion through confocal volume. This prevents spectral cross-talk *i.e.*, detection of donor photons in the acceptor-emission channel, which causes erroneous E values (Hohlbein, Craggs, and Cordes, 2014). Fluorescence bursts are then detected in a single-photon avalanche diode (SPAD) detector, and further analyzed by software for freely-diffusing smFRET data.
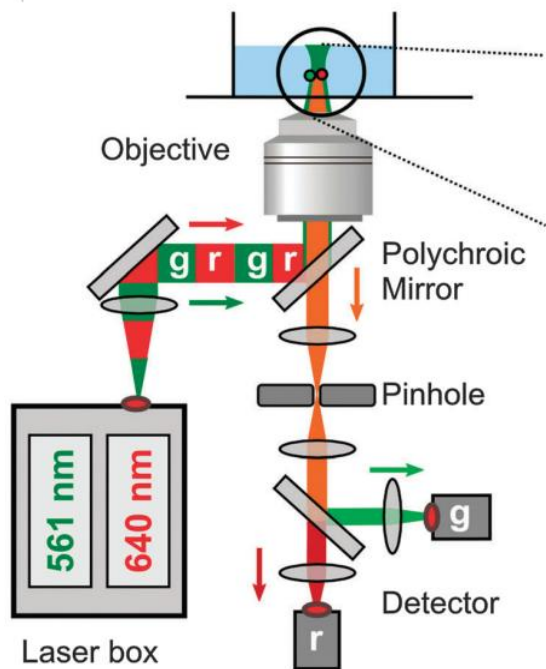
Figure 3.3: smFRET. A laser box generates green and red lights, which upon passing through a collimating lens and a polychroic mirror, focus on an objective in an epi-fluorescence configuration. After the spatial restriction of the confocal volume by the pinhole, the emitted green and red light are separated into corresponding detector channels (Hohlbein, Craggs, and Cordes, 2014).

4 Experimental Section

4.1 Materials

4.1.1 Buffer, Reagents, and Chromophores

TRIS Buffer: contained 20 µM TRIS (2-amino-2-(hydroxymethyl)propane-1,3-diol, 242.27 g/mol (PubChem)), 50 µM KCl, and 2 µM $MgCl_2$ (adjusted to pH 7.5).

ATP and ADP were used as biological effectors for observation of Sec translocon dynamics.

ATTO 565 and ATTO 643 were utilized as chromophores.

4.1.2 Proteins

SecA, SecYEG, and pSpy were used. To observe conformational changes in the SecA, site-directed mutagenesis with maleimide derivatization were done at protein positions 280, and 330 corresponding to PPXD domain; position 604 in NBD2 domain, and position 714 in HWD domain. Figure 4.1 shows the structure of the mutated SecA.
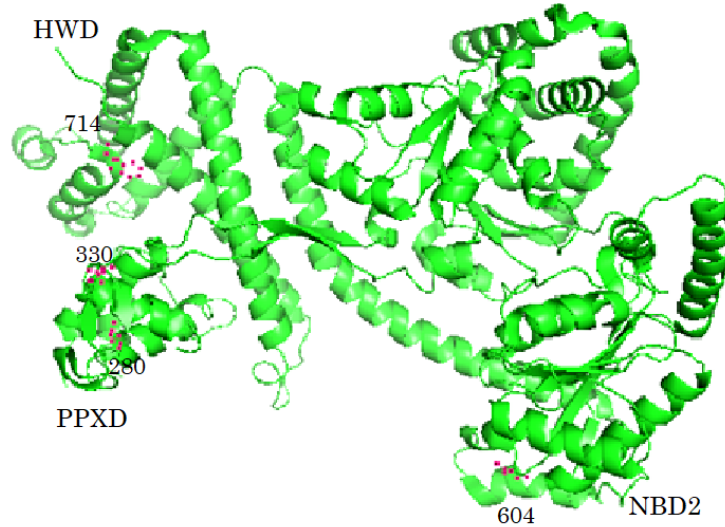
Figure 4.1: SecA. Red dots denote the induced mutations, where the left bottom ones correspond to positions 280, and 330 of the PPXD domain; the left upper ones to position 714 of the HWD domain, and the right bottom ones to the position 604 of the NBD2 domain. The image was created with Pymol.

4.2 Methods

4.2.1 Single Molecule Detection Techniques

4.2.1.1 FCS

Optimization of the diffused-based confocal system, shown in Figure 3.2, required investigation of the influence of the focal depth in fluorescence parameters, especially on molecular brightness and SNR. A scheme depicting focal depth is shown in Figure 4.2. Establishing the aim few instrumental modifications were done, such as power reduction of the laser to 75% preventing fluorescence photo-bleaching effects. The laser used generated electromagnetic radiation with a wavelength of 561 nm and a frequency of 20 MHz. The sample composition consisted of 0.1 nM ATTO 565, dissolved on a Tris buffer. The selection of the particular chromophore was made due to high fluorescence quantum yield, high thermal, and photostability qualities. Data collection was done through consecutive position changes of the microscope objective relative to the surface of the coverslip, on top of which was placed the sample containing the dye. All the data were analyzed using PicoQuant software.
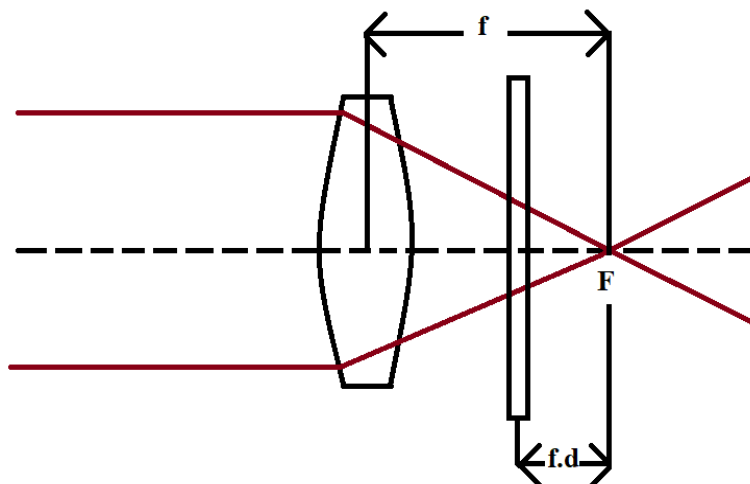
Figure 4.2: Focal Depth. Red lines denote the light, *f* the focal length, and *F* the focal point. Focal depth is designated with *f.d* which represents the distance between the focal point and the coverslip.

4.2.1.2 Ensemble FRET

Conformational changes during the addition of the ATP in the SecA protein were analyzed by ensemble FRET, using fluorimetry. Four samples were prepared to contain two modified SecA proteins; one with chromophores ATTO 565 and ATTO 643 attached to the cysteine amino acid in positions 330 (PPXD) and 714 (HWD) of its sequence, and the second with the same chromophores attached to the positions 280 (PPXD) and 604 (NBD2), respectively. The first sample prepared contained 99.5 µL TRIS buffer and 2 µL of the SecA with chromophores attached on positions 330 and 714, with initial concentration of 1 µM. On the second sample, 1 µL ATP solution was added with an initial concentration of 100 mM. The third solution was prepared by the addition of 999 µL of the buffer and 1 µL of the SecA, with chromophores attached on the positions 280 and 604, respectively; whereas in the fourth solution, 1 µL of ATP was added to the third solution. Chromophores on the samples were excited by a radiation with the corresponding maximum absorption wavelength.

14

4.2.1.3 smFRET

Modified SecA protein in positions 330 (PPXD), and 714 (HWD) were analyzed using a diffused-based smFRET confocal system, shown in Figure 3.3. In addition, SecA-SecYEG, SecA-SecYEG-ADP, and SecA-SecYEG-ATP mixtures were investigated. All samples prepared were ensured to be at a concentration smaller than 100 pM. The data were analyzed using FRETBursts, as open source software for the interpretation of freely-diffusing smFRET data (Ingargiola et al., "FRETBursts: An Open Source Toolkit for Analysis of Freely-Diffusing Single-Molecule FRET").

5 Results and Discussion

5.1 The Dependence of Fluorescence Parameters on Focal Depth Variation

The single-molecule fluorescence experimentations are highly sensitive to signal-to-noise ratio (SNR) and signal-to-background-ratio (SBR), therefore the correctly applied focal depth is of high importance. This experiment aimed to determine the influence of the focal depth in fluorescence parameters, with a distinct awareness of the molecular brightness and SNR, using a diffused-based FCS confocal system. Figure 5.1 and Figure 5.2 show the dependence of the molecular brightness, defined as the ratio of the mean photons counts per second (CPS) to the average number of molecules in the confocal volume (Yamamoto and Sasaki), and the SNR to the focal depth.
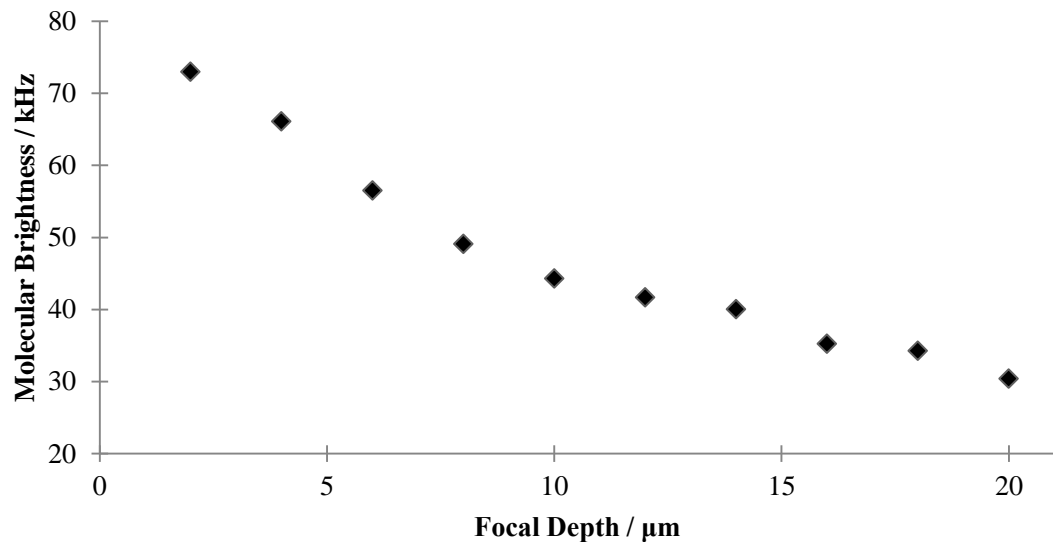

Figure 5.1: Dependence of the molecular brightness upon focal depth variation. It shows a steep increase in the molecular brightness from 10 μm, at 44 kHz, as the focal depth approaches 0 μm. The highest molecular brightness value is reached at 2 μm with 73 kHz. From 10 to 20 μm a relatively small change in molecular brightness is observed, from 44 kHz to 30 kHz, respectively.
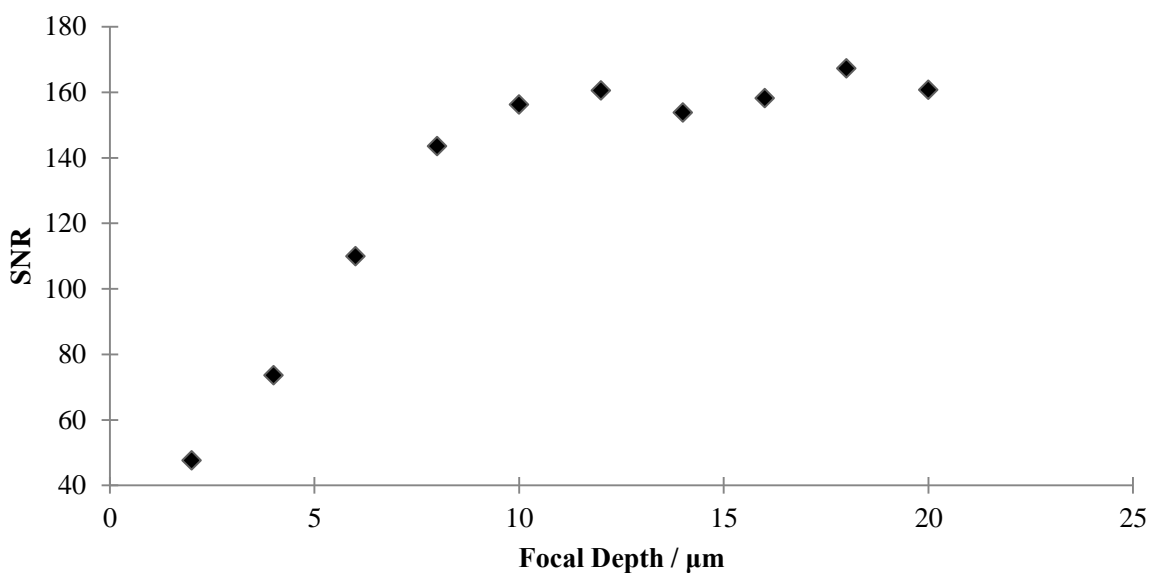
16

Figure 5.2: Dependence of the SNR upon focal depth variation. It shows a steep increase in the SNR, from 2 µm, at 48, as the focal depth reaches 10 µm, at 156. The highest SNR is reached above 10 µm with a value of around 160. From 10 to 20 µm a relatively small change in SNR is observed, from 156 to 161, respectively.

The results shown above may suggest an increase in the noise as the focal depth decreases from 10 µm to the surface of the cover-slip, and a relatively constant signal as the focal depth increases from 10 to 20 µm. This was a necessary step in the optimization of our single-molecule experiments, which led to an increase in data quality.

5.2   Ensemble FRET Measurements of Configuration Changes in SecA

5.2.1   Ensemble FRET Measurements of Configuration Changes in SecA-ATP Mixture

This experiment aimed to measure configuration changes in SecA in presence of ATP. The graphs in Figures 5.3, and 5.4 depict ensemble FRET measurements of SecA, mutated in positions 280 (PPXD), 604 (NBD2), and 330 (PPXD), 714 (HWD), respectively, alone and with the addition of ATP. Table 5.1 summarizes the relative proximity ratios (E_{PR}), which is calculated as follows:

$$E_{PR} = \frac{I(\lambda_{fl,d})}{I(\lambda_{fl,d}) + I(\lambda_{fl,a})}$$

[5.1]

where *I* denotes the fluorescence intensity, whereas $\lambda_{fl,d}$, and $\lambda_{fl,a}$, the fluorescence emission maximum of the donor, and the acceptor chromophores utilized (ATTO 643 as the donor, and ATTO 565 as the acceptor), respectively (McCann et al.).
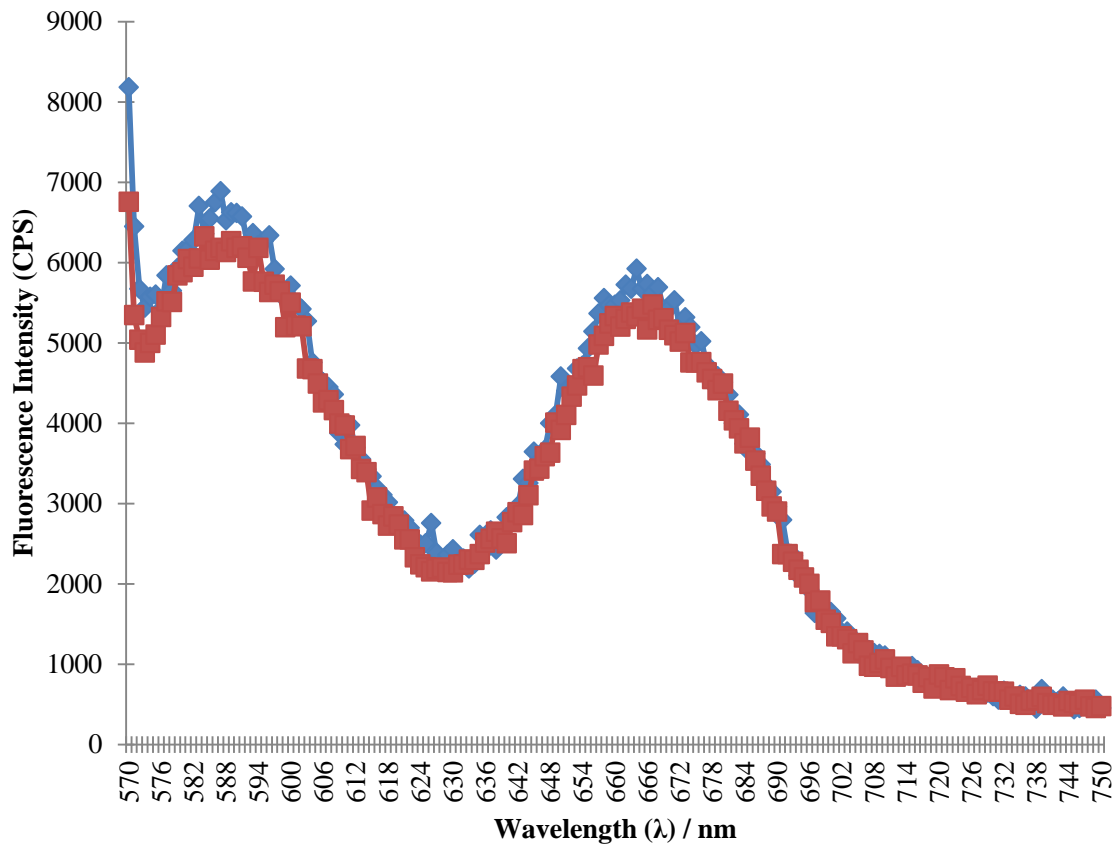

Figure 5.3: Ensemble FRET Measurements of SecA and SecA-ATP mixture. It shows the fluorescence spectrum of the ATTO 565 dye, as a donor, and ATTO 643, as the acceptor, attached to the cysteine amino acid, located on 280 (PPXD) and 604 (NBD2) positions, respectively. The first peak displays light emission from the donor, whereas the second one from the acceptor, signifying the FRET occurrence. The blue dots represent the FRET process occurring between the dyes on the SecA protein, whereas the red ones after the addition of the ATP.
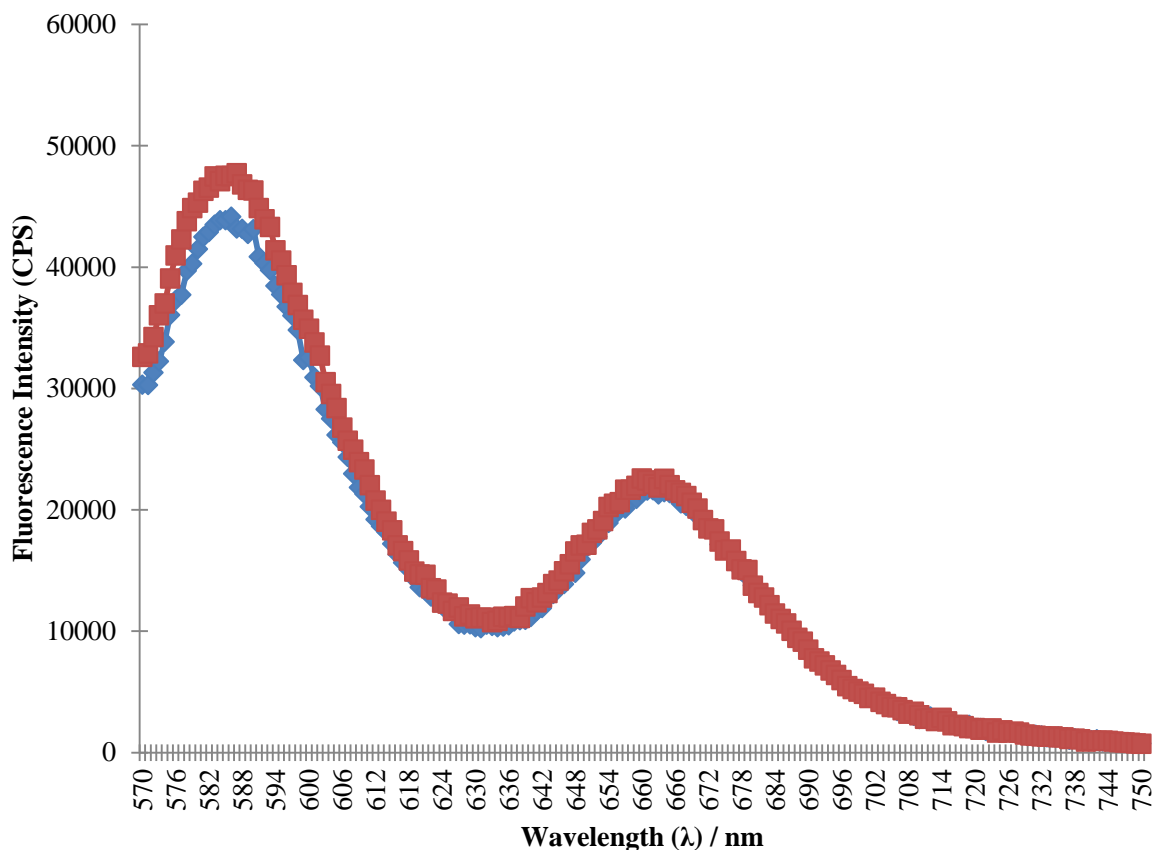
Figure 5.4: Ensemble FRET measurements of SecA and SecA-ATP mixture. It shows the fluorescence spectrum of the ATTO 565 dye, as a donor, and ATTO 643, as the acceptor, attached to the cysteine amino acid, located on 330 (PPXD) and 714 (HWD) positions, respectively. The first peak displays light emission from the donor, whereas the second one from the acceptor, signifying the FRET occurrence. The blue dots represent the FRET process occurring between the dyes on the SecA protein, whereas the red ones after the addition of the ATP.

Table 5.1: Summary of E_{PR} of the investigated samples. APO denotes the sample with only SecA protein present. The addition of ATP on the SecA mutated at positions 330 and 714, decreased E_{PR} from 0.32 to 0.33; whereas the sample mutated at positions 280 and 604 decreased it from 0.46 to 0.47.

	APO	SecA-ATP
PPXD-HWD	0.32	0.33
PPXD-NBD2	0.46	0.47

The results show almost no significant difference in the FRET after the addition of the ATP. This may suggest a limited ATPase activity of the SecA, due to the absence of the SecYEG and substrate protein (Robson et al., 2009).

5.2.2   Ensemble FRET Measurements of Configuration Changes in SecA-pSpy and SecA-pSpy-ATP Mixtures

This experiment aimed to measure configuration changes in SecA when combined with pSpy, and pSpy-ATP complex. The graphs in Figures 5.5, 5.6, and 5.7 depict ensemble FRET measurements of SecA, mutated in positions 330 (PPXD), and 714 (HWD), alone, with the addition of pSpy, and addition of the ATP on the latter sample. Table 5.2 summarizes E_{PR} values calculated from the results gained.
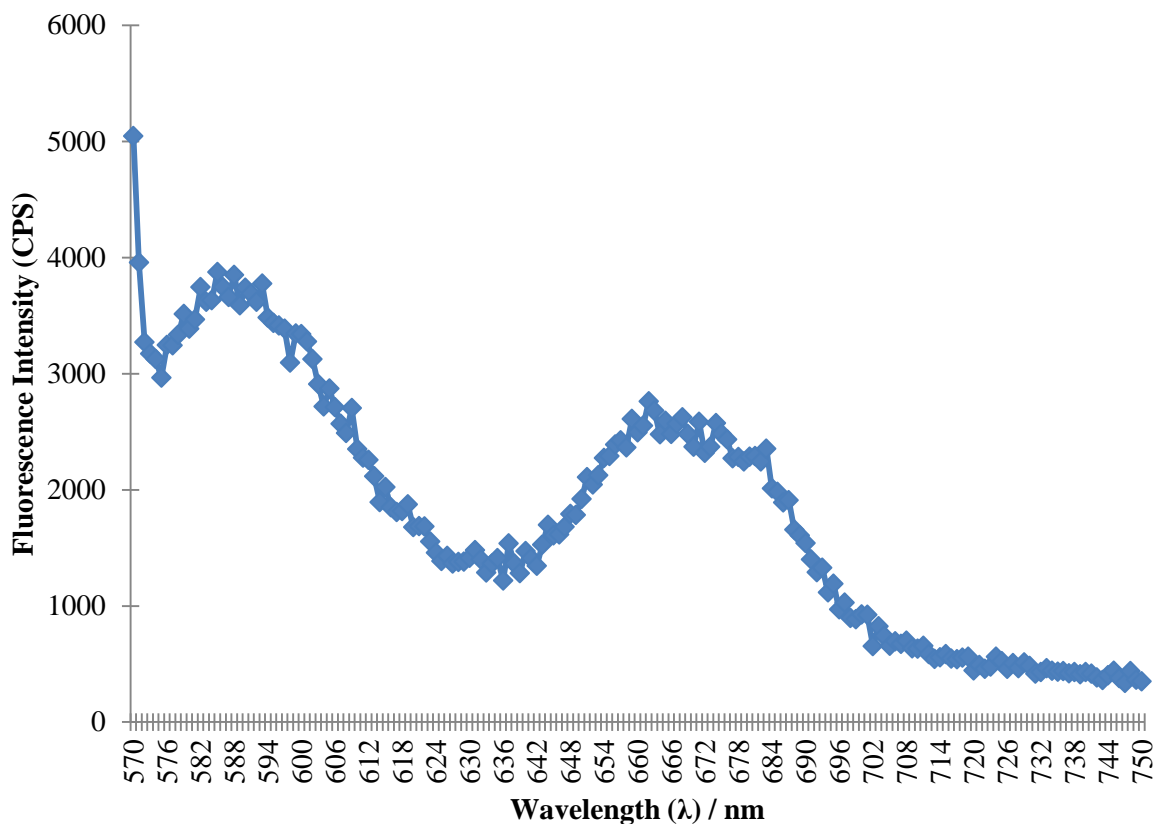
Figure 5.5: Ensemble FRET measurements of the SecA. It shows the fluorescence spectrum of the ATTO 565 dye, as a donor, and ATTO 643, as the acceptor, attached to the cysteine amino acid, located on 330 (PPXD) and 714 (HWD) positions of the SecA. The first peak displays light emission from the donor, whereas the second one from the acceptor, signifying the FRET occurrence.

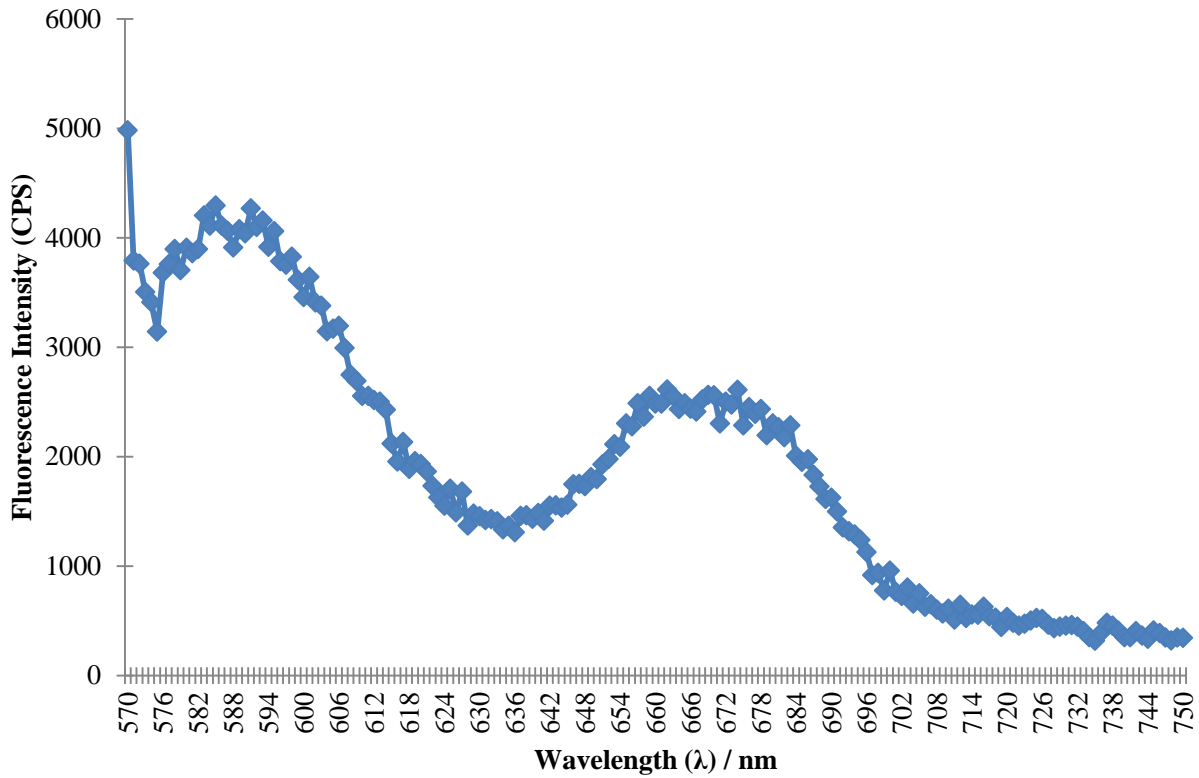Figure 5.6: Ensemble FRET Measurements of the SecA with pSpy. It shows the fluorescence spectrum of the ATTO 565 dye, as a donor, and ATTO 643, as the acceptor, attached to the cysteine amino acid, located on 330 (PPXD) and 714 (HWD) positions of the SecA with pSpy, respectively. The first peak displays light emission from the donor, whereas the second one from the acceptor, signifying the FRET occurrence.
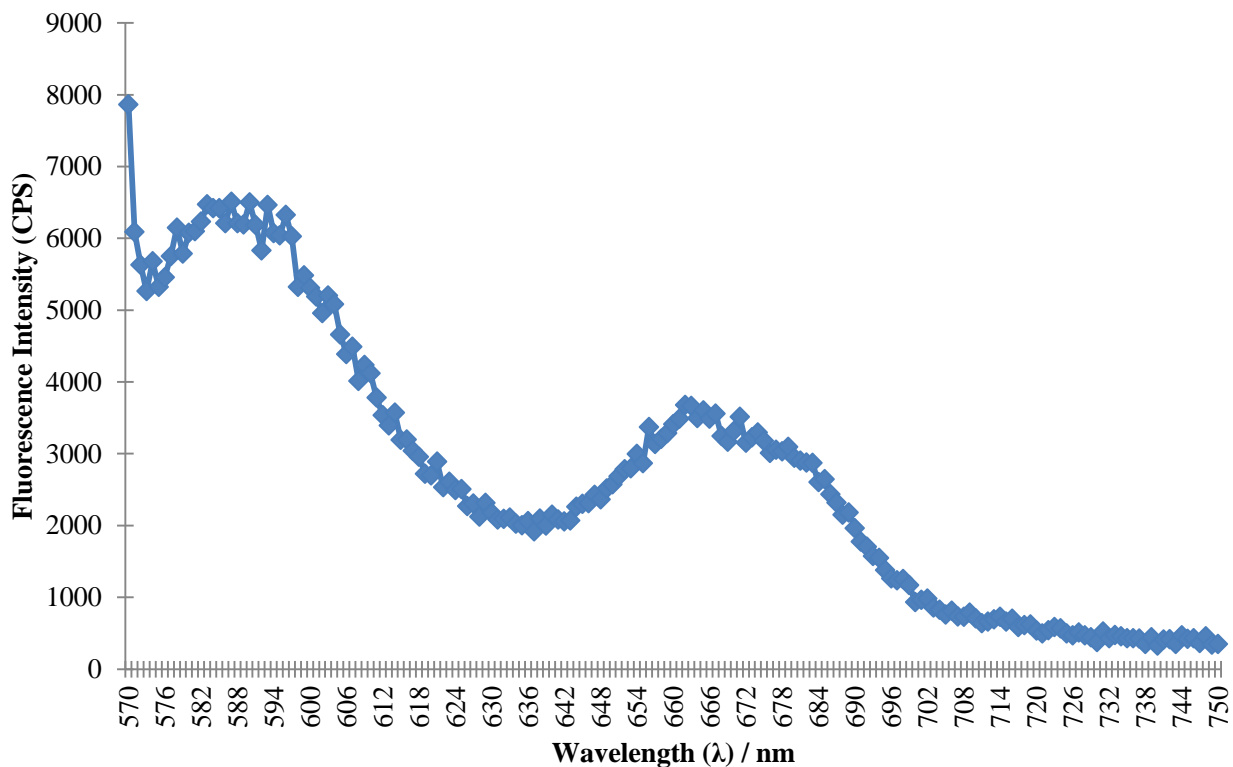
Figure 5.7: Ensemble FRET Measurements of the SecA Complexed pSpy and ATP. It shows the fluorescence spectrum of the ATTO 565 dye, as a donor, and ATTO 643, as the acceptor, attached to the cysteine amino acid, located on 330 (PPXD) and 714 (HWD) positions of the SecA with pSpy and ATP, respectively. The first peak displays light emission from the donor, whereas the second one from the acceptor, signifying the FRET occurrence.

Table 5.2: E_{PR} value summary of the investigated samples. The addition of pSpy decreases E_{PR} from 0.41 to 0.38, whereas with the addition of ATP E_{PR} reached the lowest value of 0.36.

APO PPXD-HWD	pSpy SecA PPXD-HWD	ATP pSpy SecA PPXD-HWD
0.41	0.38	0.36

The results depict a decrease in E_{PR} when pSpy and ATP were added to the SecA protein sample. This E_{PR} decrease may have been a result of an increase in distance between PPXD and HWD domains by rotational and translational movements of the SecA, which may suggest the occurrence of the "closed" conformation of the SecA. No significant decrease of E_{PR} when only pSpy was added, implying the crucial role of ATP in the function of SecA.

5.3 smFRET Measurements of Configuration Changes in SecA

This experiment aimed to measure configuration changes in SecA, upon addition of ADP, and ATP, in the presence of SecYEG. The graph in Figure 5.8 depicts smFRET measurements of SecA, mutated in positions 330 (PPXD), and 714 (HWD). In the Figure 5.9 is shown smFRET measurement for SecA coupled with SecYEG, whereas on 5.10, and 5.11, are observed effects of addition of ADP and ATP on the SecA-SecYEG mixture, respectively.
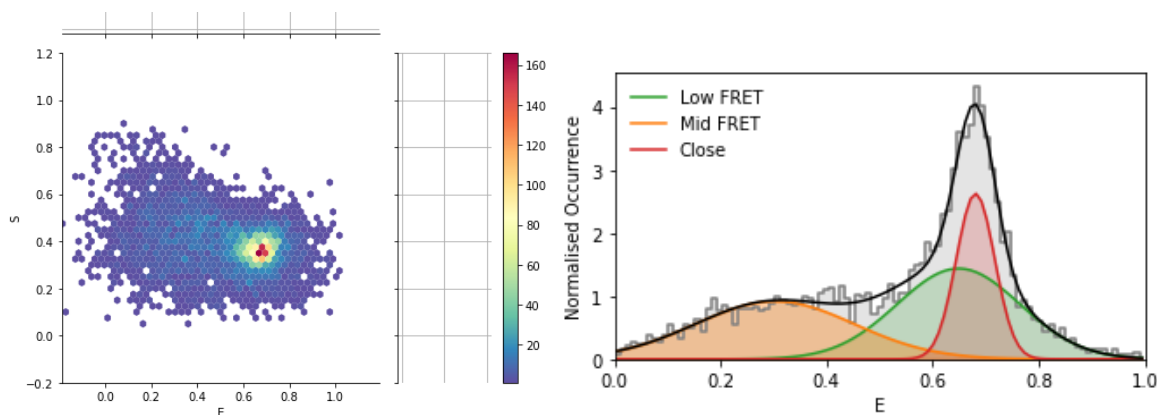

Figure 5.8: smFRET Measurement of the SecA. The first picture depicts a 2-D ALEX histogram of the SecA. The second one shows the E histogram fitted with a Gaussian model and normalized. The S value peaks at approximately 0.4. The normalized E histogram fitted with a Gaussian model shows three populations; low FRET peaking at around 0.6 E, and around 3/8 Normalised Occurrence (NO) with broad width; mid FRET peaking at around 0.3 E, and 1/4 NO with broad width; and close FRET FRET peaking at 0.7 E, and around 1/2 NO with narrow width. The sum of the fits (black curve) shows two population; one peaking at around 0.2 E, and 1/4 NO, with broad width; and the other peaking at 0.7 E, and 1 NO.
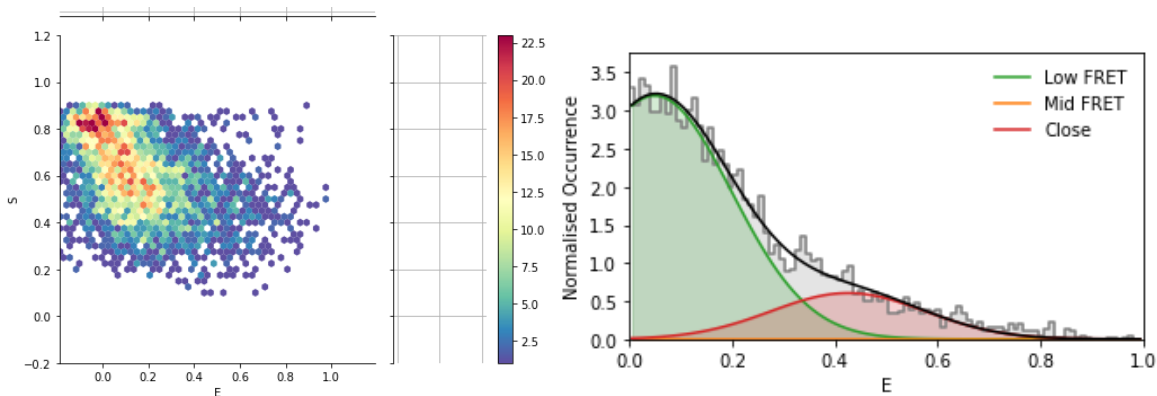
Figure 5.9: smFRET Measurement of the SecA, with SecYEG. The first picture depicts a 2-D ALEX histogram of the SecA. The second one shows the E histogram fitted with a Gaussian model and normalized. The S value peaks at a range of 0.8 to 0.9, but otherwise spread from 0.9 to around 0.5. The normalized E histogram fitted with a Gaussian model shows two populations; low FRET peaking at around 0.1 E, and around 13/14 NO with broad width; and close FRET peaking at around 0.4 E, and around 1/7 NO with broad width. The sum of the fits shows one population peaking at around 0.1 E, and 13/14 NO, with broad width.

Figure 5.10: smFRET Measurement of the SecA, with SecYEG and ADP. The first picture depicts a 2-D ALEX histogram of the SecA. The second one shows the E histogram fitted with a Gaussian model and normalized. The S value ranges from 0.7 to 0.9. The normalized E histogram fitted with a Gaussian model shows three populations; low FRET peaking at around 0.1 E, and around 3/4 NO with relatively broad width; mid FRET peaking at around 0.3 E, and around 1/8 NO with broad width; and close FRET which is almost insignificant, peaking at around 0.7 E, and around 1/20 NO with broad width. The sum of the fits shows one population peaking at around 0.1 E, and 7/8 NO, with relatively broad width.
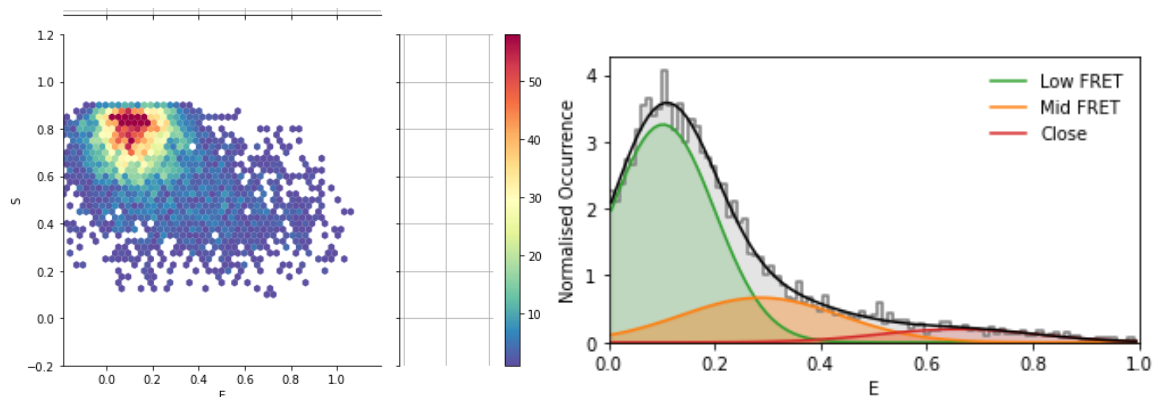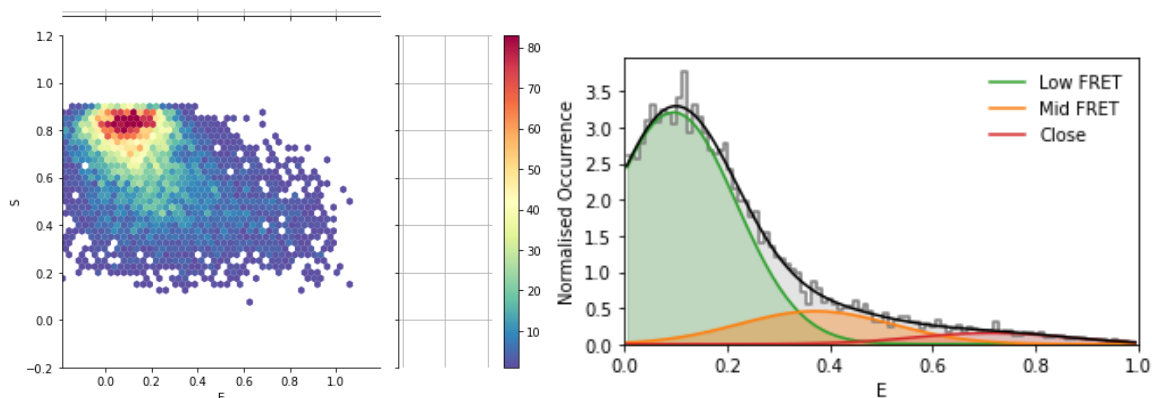
Figure 5.11: smFRET Measurement of the SecA, with SecYEG and ATP. The first picture depicts a 2-D ALEX histogram of the SecA. The second one shows the E histogram fitted with a Gaussian model and normalized. The S value ranges from 0.8 to 0.9. The normalized E histogram fitted with a Gaussian model shows three populations; low FRET peaking at around 0.1 E, and around 13/14 NO with relatively broad width; with mid FRET and close FRET peaking at around 0.4 E, 1/7 NO, and 0.7 E, 1/14 NO, which are almost insignificant. The sum of the fits shows one population peaking at around 0.1 E, and 13/14 NO, with relatively broad width.

Table 5.3: Summarized results from the smFRET measurements of the investigated samples. SecA alone showed narrow-width sum of the fits E distribution, with a value peaking at 0.7 E. When SecYEG was added the corresponding E distributions with broad width, peaking at 0.1 appeared. The addition of ADP and ATP showed an E distribution with narrower width compared to the mixture SecA-SecYEG, both peaking at 0.1.

	E	Sum of the Fits Width
SecA	0.7	narrow
SecA-SecYEG	0.1	broad
SecA-SecYEG-ADP	0.1	narrow
SecA-SecYEG-ATP	0.1	narrow

As seen by the results in Table 5.3 upon addition of the SecYEG, broad-shaped sum of fits E distributions are observed, which may indicate the presence of static heterogeneity, dynamic heterogeneity, or a combination of the two. However, upon addition of the ADP, or ATP, a narrower-width mean E is observed, thus suggesting an occurrence of a conformational change in the SecA, with an increased distance between PPXD and HWD domains. No distinction of the SecA state in the SecA-SecYEG-ADP and SecA-SecYEG-ATP mixtures was possible to observe. As all the SecA proteins were labeled with the

same donor-to-acceptor ratio (1:1), values in *S* greater, or smaller than 0.5, may suggest a steric hindrance of acceptor, or the donor, respectively; blinking of the corresponding choromophores; or photobleaching.

A summarized table regarding the observed state of the clamp of the SecA in the experimented conditions is shown on Table 5.4.

Table 5.4: State of the clamp of SecA in investigated biological conditions.

Sample	Distance Investigated	State of the Clamp
SecA	PPXD-NBD2	Open
SecA	PPXD-HWD	Open
SecA-ATP	PPXD-NBD2	Open
SecA-ATP	PPXD-HWD	Open
SecA-pSpy	PPXD-HWD	Open
SecA-pSpy-ATP	PPXD-HWD	Closed
SecA-SecYEG	PPXD-HWD	Not defined
SecA-SecYEG-ADP	PPXD-HWD	Closed
SecA-SecYEG-ATP	PPXD-HWD	Closed

6 Conclusions

Results show the best applicable focal depth is 10 μm, as this distance shows the best compromise between the highest molecular brightness and SNR.

Ensemble FRET measurements show no effect on the SecA sample upon addition of the ATP, suggesting a limited activity of the ATPase in the absence of a substrate protein, or the SecYEG complex. However, the addition of the pSpy on the SecA-ATP mixture was accompanied by a conformational change on SecA, particularly on a distance increase between PPXD and HWD domains, suggesting the formation of the 'closed' conformation. No significant conformational changes in SecA were observed when no ATP was present in the given mixture.

smFRET measurement results also support the main hypothesis from ensemble FRET measurements. However, further work should be done on improving experimental conditions such as labeling, choice of dyes, anti-photobleaching cocktail, to properly capture the conformational dynamics of SecA.

7 References

Allen, W.J., Corey, R.A., Oatley, P., Sessions, R.B., Baldwin, S.A., Radford, S.E., Tuma, R. and Collinson, I. (2016). Two-way communication between SecY and SecA suggests a Brownian ratchet mechanism for protein translocation. eLife, 5. doi:10.7554/elife.15598.

Bauer, B.W. and Rapoport, T.A. (2009). Mapping polypeptide interactions of the SecA ATPase during translocation. Proceedings of the National Academy of Sciences of the United States of America, [online] 106(49), pp.20800–20805. doi:10.1073/pnas.0910550106.

Bauer, Benedikt W., Shemesh, T., Chen, Y. and Rapoport, Tom A. (2014). A 'Push and Slide' Mechanism Allows Sequence-Insensitive Translocation of Secretory Proteins by the SecA ATPase. Cell, [online] 157(6), pp.1416–1429. doi:10.1016/j.cell.2014.03.063.

Berg, B. van den, Clemons, W.M., Collinson, I., Modis, Y., Hartmann, E., Harrison, S.C. and Rapoport, T.A. (2003). X-ray structure of a protein-conducting channel. Nature, 427(6969), pp.36–44. doi:10.1038/nature02218.

Chen, Y., Bauer, B.W., Rapoport, T.A. and Gumbart, J.C. (2015). Conformational Changes of the Clamp of the Protein Translocation ATPase SecA. Journal of Molecular Biology, [online] 427(14), pp.2348–2359. doi:10.1016/j.jmb.2015.05.003.

Cranford-Smith, T. and Huber, D. (2018). The way is the goal: how SecA transports proteins across the cytoplasmic membrane in bacteria. FEMS microbiology letters, [online] 365(11), p.fny093. doi:10.1093/femsle/fny093.

Economou, A. and Wickner, W. (1994). SecA promotes preprotein translocation by undergoing ATP-driven cycles of membrane insertion and deinsertion. Cell, [online] 78(5), pp.835–843. doi:10.1016/s0092-8674(94)90582-7.

Erlandson, K.J., Miller, S.B.M., Nam, Y., Osborne, A.R., Zimmer, J. and Rapoport, T.A. (2008). A role for the two-helix finger of the SecA ATPase in protein translocation. Nature, [online] 455(7215), pp.984–987. doi:10.1038/nature07439.

Fak, J.J., Itkin, A., Ciobanu, D.D., Lin, E.C., Song, X.-J., Chou, Y.-T., Gierasch, L.M. and Hunt, J.F.

(2004). Nucleotide exchange from the high-affinity ATP-binding site in SecA is the rate-limiting step in the ATPase cycle of the soluble enzyme and occurs through a specialized conformational state. Biochemistry, [online] 43(23), pp.7307–7327. doi:10.1021/bi0357208.

Gelis, I., Bonvin, A.M.J.J., Keramisanou, D., Koukaki, M., Gouridis, G., Karamanou, S., Economou, A. and Kalodimos, C.G. (2007). Structural Basis for Signal-Sequence Recognition by the Translocase Motor SecA as Determined by NMR. *Cell*, 131(4), pp.756–769. doi:10.1016/j.cell.2007.09.039.

Gold, V.A.M., Whitehouse, S., Robson, A. and Collinson, I. (2013). The dynamic action of SecA during the initiation of protein translocation. The Biochemical Journal, [online] 449(3), pp.695–705. doi:10.1042/BJ20121314.

Gouridis, G., Karamanou, S., Sardis, M., Schärer, M., Capitani, G. and Economou, A. (2013). Quaternary Dynamics of the SecA Motor Drive Translocase Catalysis. Molecular Cell, [online] 52(5), pp.655–666. doi:10.1016/j.molcel.2013.10.036.

Hohlbein, J., Craggs, T.D. and Cordes, T. (2014). Alternating-laser excitation: single-molecule FRET and beyond. Chem. Soc. Rev., 43(4), pp.1156–1171. doi:10.1039/c3cs60233h.

Hunt, J.F., Weinkauf, S., Henry, L., Fak, J.J., McNicholas, P., Oliver, D.B. and Deisenhofer, J. (2002). Nucleotide control of interdomain interactions in the conformational reaction cycle of SecA. Science (New York, N.Y.), [online] 297(5589), pp.2018–2026. doi:10.1126/science.1074424.

Ingargiola, Antonino, et al. "FRETBursts: An Open Source Toolkit for Analysis of Freely-Diffusing Single-Molecule FRET." PLOS ONE, vol. 11, no. 8, 17 Aug. 2016, p. e0160716, 10.1371/journal.pone.0160716. Accessed 30 Apr. 2022.

Lakowicz, Joseph R. Principles of Fluorescence Spectroscopy. New York, Springer Science+Business Media, 2010.

Li, L., Park, E., Ling, J., Ingram, J., Ploegh, H. and Rapoport, T.A. (2016a). Crystal structure of a substrate-engaged SecY protein-translocation channel. Nature, [online] 531(7594), pp.395–399. doi:10.1038/nature17163.

Li, W., Schulman, S., Boyd, D., Erlandson, K., Beckwith, J. and Rapoport, T.A. (2007b). The Plug

Domain of the SecY Protein Stabilizes the Closed State of the Translocation Channel and Maintains a Membrane Seal. Molecular Cell, 26(4), pp.511–521. doi:10.1016/j.molcel.2007.05.002.

Lill, R., Cunningham, K., Brundage, L.A., Ito, K., Oliver, D. and Wickner, W. (1989). SecA protein hydrolyzes ATP and is an essential component of the protein translocation ATPase of Escherichia coli. The EMBO journal, [online] 8(3), pp.961–966. Available at: https://www.ncbi.nlm.nih.gov/pubmed/2542029 [Accessed 20 Apr. 2020].

McCann, James J., et al. "Optimizing Methods to Recover Absolute FRET Efficiency from Immobilized Single Molecules." *Biophysical Journal*, vol. 99, no. 3, 4 Aug. 2010, pp. 961–970, www.ncbi.nlm.nih.gov/pmc/articles/PMC2913196/, 10.1016/j.bpj.2010.04.063.

Miller, Helen, et al. "Single-Molecule Techniques in Biophysics: A Review of the Progress in Methods and Applications." Reports on Progress in Physics, vol. 81, no. 2, 19 Dec. 2017, p. 024601, 10.1088/1361-6633/aa8a02. Accessed 28 Aug. 2019.

Nishiyama, K., Hanada, M. and Tokuda, H. (1994). Disruption of the gene encoding p12 (SecG) reveals the direct involvement and important function of SecG in the protein translocation of Escherichia coli at low temperature. The EMBO Journal, 13(14), pp.3272–3277. doi:10.1002/j.1460-2075.1994.tb06628.x.

Oliver, D.B. and Beckwith, J. (1981). E. coli mutant pleiotropically defective in the export of secreted proteins. Cell, [online] 25(3), pp.765–772. doi:10.1016/0092-8674(81)90184-7.

Oliver, D.B. and Beckwith, J. (1982). Identification of a new gene (secA) and gene product involved in the secretion of envelope proteins in Escherichia coli. Journal of Bacteriology, [online] 150(2), pp.686–691. Available at: https://www.ncbi.nlm.nih.gov/pubmed/6279567 [Accessed 4 Mar. 2020].

Pawley, James B, and Springer Science+Business Media. Handbook of Biological Confocal Microscopy. New York, Springer, [Post, 2007].

Schiebel, E., Driessen, A.J., Hartl, F.U. and Wickner, W. (1991). Delta mu H+ and ATP function at different steps of the catalytic cycle of preprotein translocase. Cell, [online] 64(5), pp.927–939. doi:10.1016/0092-8674(91)90317-r.

Schmidt, M.G., Rollo, E.E., Grodberg, J. and Oliver, D.B. (1988). Nucleotide sequence of the secA gene

and secA(Ts) mutations preventing protein export in Escherichia coli. Journal of Bacteriology, [online] 170(8), pp.3404–3414. doi:10.1128/jb.170.8.3404-3414.1988.

Taura, T., Baba, T., Akiyama, Y. and Ito, K. (1993). Determinants of the quantity of the stable SecY complex in the Escherichia coli cell. Journal of Bacteriology, [online] 175(24), pp.7771–7775. Available at: https://www.ncbi.nlm.nih.gov/pmc/articles/PMC206951/ [Accessed 20 Apr. 2020].

van der Wolk, J.P.W. (1997). The catalytic cycle of the Escherichia coli SecA ATPase comprises two distinct preprotein translocation events. The EMBO Journal, 16(24), pp.7297–7304. doi:10.1093/emboj/16.24.7297.

Volkhard Helms. Principles of Computational Cell Biology : From Protein Complexes to Cellular Networks. Weinheim, Wiley-Vch, 2008.

Yamamoto, Johtaro, and Akira Sasaki. "Measurement of the Concentration and the Brightness for Samples Containing Multiple Molecules with Different Brightness Using Fluorescence Correlation Spectroscopy." Applied Sciences, vol. 11, no. 13, 23 June 2021, p. 5840, 10.3390/app11135840. Accessed 12 May 2022.

Ye, J., Osborne, A.R., Groll, M. and Rapoport, T.A. (2004). RecA-like motor ATPases—lessons from structures. Biochimica et Biophysica Acta (BBA) - Bioenergetics, [online] 1659(1), pp.1–18. doi:10.1016/j.bbabio.2004.06.003.

Yu, Lan, et al. "A Comprehensive Review of Fluorescence Correlation Spectroscopy." Frontiers in Physics, vol. 9, 12 Apr. 2021, 10.3389/fphy.2021.644450. Accessed 28 Apr. 2022.

Zimmer, J., Nam, Y. and Rapoport, T.A. (2008). Structure of a complex of the ATPase SecA and the protein-translocation channel. Nature, 455(7215), pp.936–943. doi:10.1038/nature07335.